Chinese Chemical Letters 35 (2024) 109403

Contents lists available at ScienceDirect

Chinese Chemical Letters

journal homepage: www.elsevier.com/locate/cclet

Highly reversible photomodulated hydrosoluble stiff-stilbene supramolecular luminophor induced by cucurbituril

Guoxing Liu[a,*], Yixin Li[a,b], Changming Tian[a], Yongmei Xiao[b], Lijie Liu[a], Zhanqi Cao[a], Song Jiang[a], Xin Zheng[a], Caoyuan Niu[a], Yun-Lai Ren[a], Liangru Yang[b], Xianfu Zheng[a], Yong Chen[c]

[a] College of Science, Henan Agricultural University, Zhengzhou 450002, China
[b] College of Chemistry and Chemical Engineering, Henan University of Technology, Zhengzhou 450001, China
[c] College of Chemistry, State Key Laboratory of Elemento-Organic Chemistry, Nankai University, Tianjin 300071, China

ARTICLE INFO

Article history:
Received 5 September 2023
Revised 5 December 2023
Accepted 14 December 2023
Available online 22 December 2023

Keywords:
Host-guest complexation
Cucurbituril
Fluorescence switch
Stiff-stilbene
Fluorescence enhancement

ABSTRACT

A photochromic molecular rotor based on stiff-stilbene (SSB-FMR) was handily prepared through coupled reaction, and further self-assembled with cucurbit[8]uril (CB[8]) to form a 2:2 quaternary supramolecular complex (SSB-FMR/CB[8]). Significantly, the intervention of CB[8] on SSB-FMR achieved dual functions that assembly-induced emission enhancement and assembly-induced improvement of photoisomerized performance (especially reversibility) of stiff-stilbene molecular photoswitch. The supramolecular strategy further facilitated the assembly as a photoresponsive fluorescence switch with outstanding fatigue resistance, which was expediently applied in high-security-level QR code anti-counterfeiting and controllable lysosome targeted imaging. The study unprecedentedly provides a supramolecular method for highly efficiently improving photoisomerized performance especially reversibility of molecular photoswitches based on stiff-stilbene, and is of vital significance for the construction of intelligent materials with excellent capability.

Stimulation response exists widely in nature. For imitating nature, a variety of stimuli-responsive intelligent systems have been constructed and aroused growing attention from researchers for application in drug delivery [1,2], microrobots and nanorobots [3], printing devices [4], liquid crystals [5], tissue engineering [6], intelligent photoluminescence [7–11], molecular machines [12,13] *etc.* In general, to endow their modulated function, the fabrication of these systems requires to import a number of stimulus-responsive groups. Among numerous stimulating factors such as acid-bases, temperature, pressure, host and guest, redox, magnetism, light seems to be an ideal stimulus as it can be delivered with high spatiotemporal precision, light of a specific wavelength can be selected, and no chemical waste is produced in the system [14]. Therefore, rational introduction of photoactive units is greatly essential and crucial for successful construction of photoinduced intelligent systems. Undoubtedly, supramolecular noncovalent complexation becomes a simple and convenient way for developing the systems, which can avoid complicated and fussy synthetic procedures. All sorts of molecular photoswitches have been handily incorporated to prepare photoinduced supramolecular materials *via* host-guest complexation, electrostatic interaction, hydrophobic effect and so on [15–17]. Among the nowadays most frequently studied and utilized photoswitches are azobenzene, stilbene, diarylethene, spiropyran, and hydrazone [18–20]. Stiff-stilbene molecular switches can undergo a large geometrical conversion upon reversible isomerization between (*Z*)- and (*E*)-configuration upon distinct ultraviolet light, and was extensively utilized to fabricate intelligent supramolecular and biological systems [21–23]. However, many of the reported stiff-stilbene derivatives do not have satisfying photoisomerized reversibility [24–27], which is a current problem that needs to be urgently addressed, as far as we know. In consequence, it is of great significance but challenging to precisely and effectively improve the photoisomerization fatigue resistance of stiff-stilbene. To date, the inclusion of macrocyclic hosts has been used to modulate photoisomerization behaviors of molecular photoswitches such as diarylethene [28,29]. These successes indicate that it is feasible to employ macrocycle-based supramolecular assembly strategies to ameliorate photoisomerized performance of stiff-stilbenes, making them more comfortable with the material functions. However, so far, the strategies using host-guest complexation to inhibit photodecomposition

* Corresponding author.
E-mail address: gxliu@henau.edu.cn (G. Liu).

https://doi.org/10.1016/j.cclet.2023.109403
1001-8417/

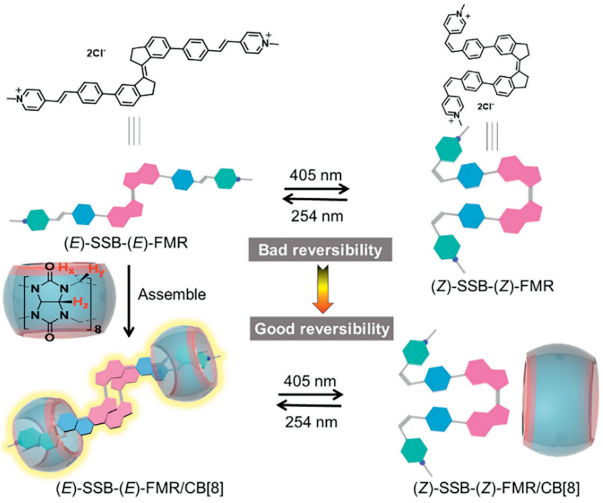

Scheme 1. Schematic illustration of assembling patterns and photo-regulation behaviors of guest SSB-FMR and host CB[8].

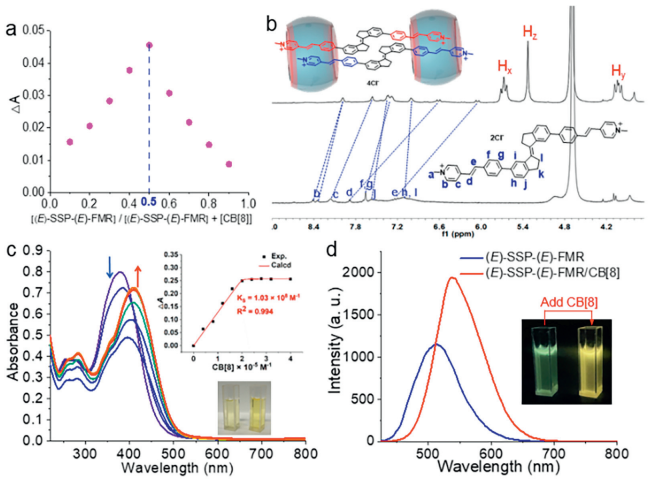

Fig. 1. (a) Host-guest binding stoichiometry of (*E*)-SSB-(*E*)-FMR with CB[8]. Job plot for the complexation of (*E*)-SSB-(*E*)-FMR with CB[8] in water at 25 °C. Absorption changes recorded at 408 nm for (*E*)-SSB-(*E*)-FMR. The sum of the total concentrations of hosts and guests was kept constant (2×10^{-5} mol/L). (b) ^{1}H NMR spectral contrast of (*E*)-SSB-(*E*)-FMR and (*E*)-SSB-(*E*)-FMR/CB[8]. (c) UV–vis titration spectra of (*E*)-SSB-(*E*)-FMR (2×10^{-5} mol/L) upon addition of CB[8] ((0~4) $\times 10^{-5}$ mol/L) in water. Inset: Nonlinear least-squares fit of the absorbance changes (ΔA) at 408 nm to determine the complex stability constant (K_S) as 1.14×10^8 L/mol; The color change of (*E*)-SSB-(*E*)-FMR (left) and assembly (*E*)-SSB-(*E*)-FMR/CB[8] (right) in water. (d) Fluorescence spectra of (*E*)-SSB-(*E*)-FMR and assembly (*E*)-SSB-(*E*)-FMR/CB[8]; Inset: fluorescence photographs of (*E*)-SSB-(*E*)-FMR and assembly (*E*)-SSB-(*E*)-FMR/CB[8] under 365 nm UV light ($\lambda_{ex} = 400$ nm).

photochromic molecules particularly stiff-stilbenes and accurately improve its photoswitching reversibility have not been reported, to the best of our knowledge.

In this work, a stiff-stilbene fluorescence molecular rotor (SSB-FMR) was prepared (Scheme 1), which could not only conduct photoisomerization between (*E*)- and (*Z*)-configuration but also possess aggregation-induced emission enhancement (AIEE). Because of introducing FMR segments, the photochromic molecular rotor could self-assemble with CB[8] to form a supramolecular assembly SSB-FMR/CB[8] *via* host-guest complexation [30]. The ingenious design that rational incorporation of CB[8] probably achieved dual functions of assembly-induced fluorescence enhancement and assembly-induced photoisomerization improvement for SSB-FMR.

(*E*)-SSB-(*E*)-FMR and (*Z*)-SSB-(*E*)-FMR were prepared through several steps (Scheme S1 in Supporting information), and their specific synthesis and characterizations are shown in Supporting information. As is well-known, CB[8] can encapsulate one or two right-sized guests with positive charge located in terminal position into its rigid cavity [31]. (*E*)-SSB-(*E*)-FMR with the feature could hopefully complex with CB[8] to form supramolecular assembly (*E*)-SSB-(*E*)-FMR/CB[8]. A reference compound FMR was prepared and its assembling behaviors with CB[8] were subsequently examined. As shown in Fig. S1 (Supporting information), an apparent upfield shift of the resonance for all the protons ($H_{a'}$-$H_{h'}$) on FMR were presented upon addition of 0.5 equiv. CB[8], suggesting that FMR was encapsulated in the cavity of CB[8]. Furthermore, when CB[8] was added into the FMR solution, the absorbance at 342 nm decreased and meanwhile, a new absorption band between 430 nm and 750 nm appeared (Fig. S2 in Supporting information), implying the generation of an intermolecular charge transfer (CT) complex. The aforementioned two proofs gave us the assembly model of FMR and CB[8] that the two guests are parallel head to tail in the cavity of CB[8], as manifested in inset of Fig. S1. Moreover, it was interesting that fluorescence intensity of FMR was greatly enhanced by a factor of up to 4.2 and maximum emission wavelength generated bathochromic shift from 427 nm to 474 nm with addition of 0.5 equiv. CB[8] (Fig. S3 in Supporting information).

Then, the successful assembly of FMR with CB[8] inspired us to further study the assembling behaviors of (*E*)-SSB-(*E*)-FMR with CB[8]. As displayed in Fig. 1a, a Job plot for the complexation of (*E*)-SSB-(*E*)-FMR with CB[8] revealed 1:1 host–guest stoichiometry, exhibiting a peak at molar fraction 0.5. By a ^{1}H NMR spectral comparison of (*E*)-SSB-(*E*)-FMR and the sample containing (*E*)-SSB-(*E*)-FMR and equivalent CB[8] (Fig. 1b), the protons (H_b-H_g) on FMR segments displayed obvious upfield shifts, indicating these parts were located in the cavity of CB[8]. Furthermore, absorption maximum of (*E*)-SSB-(*E*)-FMR manifested apparent bathochromic shift from 380 nm to 408 nm with the change in absorbance upon sequential addition of CB[8] and simultaneously, the color of (*E*)-SSB-(*E*)-FMR aqueous solution was changed from light yellow to deep yellow (Fig. 1c and Fig. S4 in Supporting information), implying occurrence of assembling behaviors between (*E*)-SSB-(*E*)-FMR and CB[8]. The absorption band between 430 nm and 750 nm which appeared in the assembly composed of FMR and CB[8] disappeared in UV–vis spectrum of the sample containing (*E*)-SSB-(*E*)-FMR and CB[8], implying that their assembling models were different. Based on UV–vis absorption spectral titration above, the complex stability constant (K_S) was determined to be 1.14×10^8 L/mol (Fig. 1c, inset), where the absorbance changes upon stepwise addition of CB[8] to the aqueous solution of (*E*)-SSB-(*E*)-FMR were analyzed by using the nonlinear least-squares fitting method [32]. To further ascertain their assembling behaviors, DOSY-NMR spectra were subsequently performed to investigate which model (polymers, oligomers or small-size supramolecular assemblies) was formed by (*E*)-SSB-(*E*)-FMR and CB[8]. As shown in Fig. S5 and Table S1 (Supporting information), diffusion coefficients of (*E*)-SSB-(*E*)-FMR/CB[8] (2.04×10^{-10} m^2/s) and (*E*)-SSB-(*E*)-FMR (2.21×10^{-10} m^2/s) were obtained through their DOSY-NMR spectra. According to the Stokes–Einstein equation ($D = kBT/(6p\eta R)$) [33], the average size of the assembly (*E*)-SSB-(*E*)-FMR/CB[8] was estimated to be equal to (*E*)-SSB-(*E*)-FMR and 3 times sum of CB[8] by assuming the complexes as being hydrodynamically spherical. Diffusion coefficients of the assembly also didnot change significantly along with change of its concentration (Table S1 and Fig. S5), which implied that (*E*)-SSB-(*E*)-FMR/CB[8] was a small-size supramolecular complex. ^{1}H–^{1}H ROESY of the (*E*)-SSB-(*E*)-FMR/CB[8] assembly (Fig. S6 in Supporting information) showed that proton correlations of $H_{f,g}$–$H_{h,i}$ and $H_{h,i}$–H_e between two adjacent (*E*)-SSB-(*E*)-FMR molecules, indicating that pyridine fraction of one guest molecule and styrene part of the other guest molecule were ar-

ranged in parallel in the cavity of CB[8] and giving a rational assembling pattern (Fig. 1b). Moreover, the ESI-MS of the assembly revealed two charge states including 3^+ and 4^+ (Fig. S7 in Supporting information). These evidences all proved that (*E*)-SSB-(*E*)-FMR and CB[8] formed a 2:2 quaternary supramolecular complex (Scheme 1). (*E*)-SSB-(*E*)-FMR and CB[8], unlike the reference compound FMR, tended to form 2:2 complex due to its suitable molecular rigidity, angles between building-blocks and linker length [34,35].

In addition, another evidence came from DLS result that average hydrodynamic radius of (*E*)-SSB-(*E*)-FMR/CB[8] was determined to be *ca.* 4.4 nm (Fig. S8 in Supporting information), which was slightly larger than two molecular size of CB[8]. This was further verified by tyndall effect of (*E*)-SSB-(*E*)-FMR/CB[8] that very faint light paths are produced irradiated by laser light (Fig. S9 in Supporting information), which implied that (*E*)-SSB-(*E*)-FMR/CB[8] should be very small nanostructures. Therefore, we speculated reasonably that (*E*)-SSB-(*E*)-FMR and CB[8] should form a simple 2:2 "head-to-head" style supramolecular assembly, as revealed in Scheme 1. Notably, when equivalent CB[8] was added in the (*E*)-SSB-(*E*)-FMR aqueous solution, its fluorescence intensity was enhanced to a certain extent and emission maximum manifested bathochromic-shift by 30 nm (from 509 nm to 539 nm) along with fluorescence color change from green to yellow attributed to the formation of a new CB[8]-stabilized charge-transfer state (Fig. 1d and Fig. S10 in Supporting information) [35]. Significantly, photoluminescence quantum yield (PLQY) of the (*E*)-SSB-(*E*)-FMR/CB[8] assembly was 0.18 greatly higher than the simple guest (*E*)-SSB-(*E*)-FMR (0.062), attributed to restriction of intramolecular rotation (RIR) caused by host-guest complexation (Fig. S11 in Supporting information). The aforementioned advantages (such as excellent photoluminescence performance and good water solubility and biocompatibility) enabled the (*E*)-SSB-(*E*)-FMR/CB[8] supramolecular assembly hopefully as a bioimaging agent.

Generally, stiff-stilbene photoswitches can undergo photoisomerization between (*E*)- and (*Z*)-configuration, which generally both requires higher energy UV light, but many of them possessed unsatisfied reversibility. Owing to the introduction of SSB unit, photoisomerized behaviors of the guest (*E*)-SSB-(*E*)-FMR and assembly (*E*)-SSB-(*E*)-FMR/CB[8] were subsequently investigated. As discerned in Fig. 2a, the absorbance of (*E*)-SSB-(*E*)-FMR at 370 nm gradually decreased, while the absorbance at 260 nm was enhanced with an isobestic point at 284 nm upon irradiation at 405 nm visible light. The new generated compound should be its (*Z*)-configuration *i.e.*, (*Z*)-SSB-(*Z*)-FMR but not (*Z*)-SSB-(*E*)-FMR, and the terrible thing was that some by-products similar to aldehydes are produced (Fig. S12 in Supporting information). Therefore, subsequent irradiation of the resultant sample at 254 nm light induced absorption spectra to partly restore (Fig. 2b). It was natural that four cyclic tests of the guest SSB-FMR suggested very unsatisfied reversibility (Fig. 2c). To further confirm the product of (*E*)-SSB-(*E*)-FMR after 405 nm light irradiation, UV–vis absorption spectral evolution of its isomer (*Z*)-SSB-(*E*)-FMR was investigated upon irradiation at 405 nm and 254 nm light. As manifested in Fig. S13a (Supporting information), when (*Z*)-SSB-(*E*)-FMR was irradiated at 405 nm light, its absorbance at 364 nm was drastically decreased and meanwhile, the absorbance at 260 nm, which was consistent with the rising absorption peak of the irradiated sample of (*E*)-SSB-(*E*)-FMR by 405 nm light, was gradually enhanced, implying the generation of the same photoproduct, *i.e.*, (*Z*)-SSB-(*Z*)-FMR. Besides, the irradiated products of (*Z*)-SSB-(*E*)-FMR by 405 nm and 254 nm light were confirmed by ^{1}H NMR spectral examination (Fig. S14 in Supporting information), which was almost identical with the ^{1}H NMR spectra of the resultant sample of (*E*)-SSB-(*E*)-FMR after irradiation at 405 nm light and 254 nm (Fig. S12), and there were some by-products similar to aldehydes presented in this system as well. Therefore, the initial spectrum of (*Z*)-SSB-(*E*)-FMR could not be completely restored and bad reversibility was revealed (Fig. S13b).

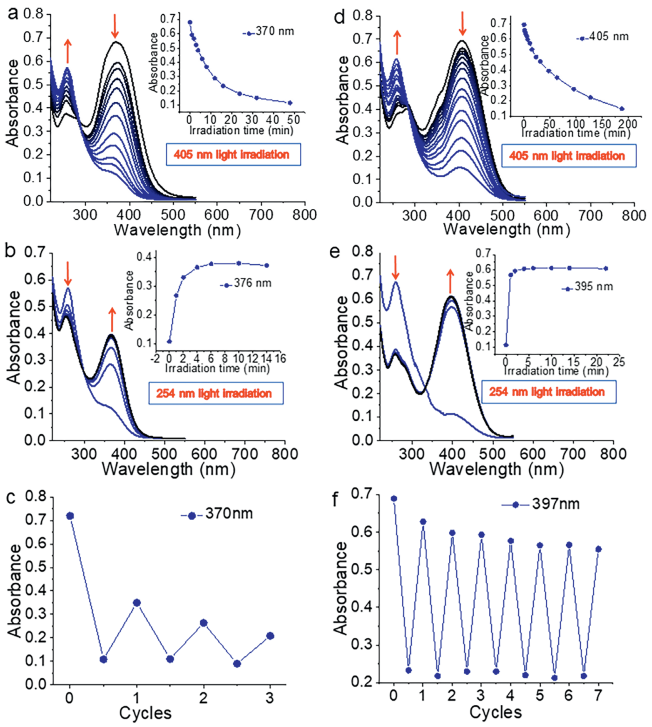

Fig. 2. (a) UV–vis spectral variation of (*E*)-SSB-(*E*)-FMR (2.0×10^{-5} mol/L) upon 405 nm light irradiation; Inset: Variation curve of the absorbance at 370 nm with increasing 405 nm irradiation time. (b) UV–vis spectral variation of the resultant sample **a** (2.0×10^{-5} mol/L) upon 254 nm light irradiation; Inset: Variation curve of the absorbance at 376 nm with increasing 254 nm irradiation time. (c) The absorbance changes at 370 nm for (*E*)-SSB-(*E*)-FMR observed upon alternating visible-light (405 nm) and UV (254 nm) irradiation. (d) UV–vis spectral variation of (*E*)-SSB-(*E*)-FMR/CB[8] (2.0×10^{-5} mol/L) upon 405 nm light irradiation; Inset: Variation curve of the absorbance at 405 nm with increasing 405 nm irradiation time. (e) UV–vis spectral variation of the resultant sample **d** (2.0×10^{-5} mol/L) upon 254 nm light irradiation; Inset: Variation curve of the absorbance at 395 nm with increasing 254 nm irradiation time. (f) The absorbance changes at 397 nm for (*E*)-SSB-(*E*)-FMR/CB[8] observed upon alternating visible-light (405 nm) and UV (254 nm) irradiation.

Next, when the supramolecular assembly (*E*)-SSB-(*E*)-FMR/CB[8] was irradiated at 405 nm, the similar phenomena as the only guest occurred in UV–vis absorption spectra that the absorbance at 405 nm declined and meanwhile absorbance at 258 nm increased, implying the formation of its isomer (*Z*)-SSB-(*Z*)-FMR/CB[8] (Fig. 2d). Nevertheless, further photoirradiation of this sample containing (*Z*)-SSB-(*Z*)-FMR/CB[8] using 254 nm light led to complete recovery of the original UV–vis absorption spectrum (Fig. 2e), manifesting that the irradiated product was re-transformed to the original substance *i.e.*, (*E*)-SSB-(*E*)-FMR/CB[8]. Crucially, the supramolecular photoswitch showed excellent fatigue resistance and no apparent recession could be observed even after repeating the cycles for at least seven times (Fig. 2f), indicating reversible photoisomerization between the (*E*)- and the (*Z*)-isomer as illustrated in Scheme 1. When 0.5 equiv. of CB[8] assembled with (*E*)-SSB-(*E*)-FMR, the possible supramolecular complex (*E*)-SSB-(*E*)-FMR/CB[8] (0.5) formed was displayed in Scheme S2 (Supporting information), which was proved by ^{1}H NMR titration (Fig. S15 in Supporting information). Its photo-switching reversibility was superior to that of the only guest and inferior to (*E*)-SSB-(*E*)-FMR/CB[8] (Fig. S16 in Supporting information), which further confirmed that CB[8] effectively improve the photoisomerization reversibility of the guest. The outstanding reversibility was further

demonstrated by ^{1}H NMR spectral evolution induced by light (Fig. S17 in Supporting information). Therefore, it is very interesting and significant that introduction of CB[8] inhibited photodecomposition of the stiff-stilbene derivative, and improved efficiently its photoisomerization reversibility. The influence of CB[6] and CB[7] on the photoisomerization of the guest were also studied (Figs. S18 and S19 in Supporting information), exhibiting that the introduction of the two CBs also could improve the photoswitching reversibility of SSB-FMR to some extent but not as good as CB[8]. In addition, CB[6] could enhance greatly the fluorescence of (*E*)-SSB-(*E*)-FMR and induce hypochromatic shift of the maximum emission peak (Fig. S20 in Supporting information). Differently, CB[7] had little effect on the fluorescence of the guest (Fig. S20).

Further structural information for (*E*)-SSB-(*E*)-FMR/CB[8] before and after 405 nm light irradiation came from transmission electron microscopy (TEM), scanning electron microscope (SEM), tyndall effect and dynamic light scattering (DLS) experiments. As shown in Fig. S6, when the (*E*)-SSB-(*E*)-FMR/CB[8] assembly was irradiated by 405 nm light, its average hydrodynamic radius underwent tremendous changes from *ca.* 4.4 nm to 690.1 nm determined by DLS. Such huge particle diameter changes revealed that a new aggregate formed after irradiation at 405 nm light. To further affirm the structure of the new aggregate, ADA was selected to perform guest competition experiment (Fig. S21 in Supporting information), where no absorption spectral variation was observed, implying that there were no binding behavior between (*Z*)-SSB-(*Z*)-FMR and CB[8]. These nanostructures should be formed by self-aggregation of (*Z*)-SSB-(*Z*)-FMR. Moreover, tyndall effect experiments gave us an intuitionistic evidence that an very apparent light path appeared for (*E*)-SSB-(*E*)-FMR/CB[8] after 405 nm light irradiation by laser light (Fig. S9), implying generation of some large nanoaggregates. Visually, the TEM and SEM images gave a clear insight into the size and shape of the (Z)-SSB-(*Z*)-FMR self-aggregates. From the TEM image (Fig. S22 in Supporting information), we could find a sphere-like nanostructure with an average diameter of 502 nm, which was further proved by SEM that a number of spherical nanoparticles were observed (Fig. S23 in Supporting information).

The above investigations inspired us to inspect whether its fluorescence could be modulated by distinct light. Interestingly, when irradiated at 405 nm light for 92 min, fluorescence emission maximum intensity of (*E*)-SSB-(*E*)-FMR/CB[8] at 539 nm was strongly quenched by 78% (Fig. 3a). Intuitively, strong yellow fluorescence turned to be dark through fluorescence photograph under 365 nm UV light (Fig. 3d). Subsequently, the quenched fluorescence intensity and photograph (under 365 nm light) of the resultant irradiated sample above were further thoroughly regained to its original level upon continuous irradiation at 254 nm light for 170 s (Figs. 3b and d). Significantly, the above light-driven fluorescence switching cycle was repeatable for at least four times without any apparent deterioration as a result of excellent photoreaction reversibility (Fig. 3c).

In view of outstanding fluorescence photoswitching performance, the photo-modulated fluorescence supramolecular assembly encouraged us to further excavate its applications. The aqueous solution containing (*E*)-SSB-(*E*)-FMR with green fluorescence was filled in the groove of special 3D model fabricated by 3D printer, showing well-defined QD code under 365 nm UV light (Fig. 3e). We could recognize the corresponding websites with our mobile phones from the green fluorescent QR code. Interestingly, the green fluorescence of QR code turned to be yellow upon addition of CB[8] attributed to the formation of (*E*)-SSB-(*E*)-FMR/CB[8]. Subsequently, irradiation at 405 nm visible light of the sample led to the strong yellow fluorescence quenching and the disappearance of QR code, which we could not recognize the corresponding website from. Crucially, when irradiated by 254 nm light, the original QR code image reemerged and was recognized by mobile phones. The

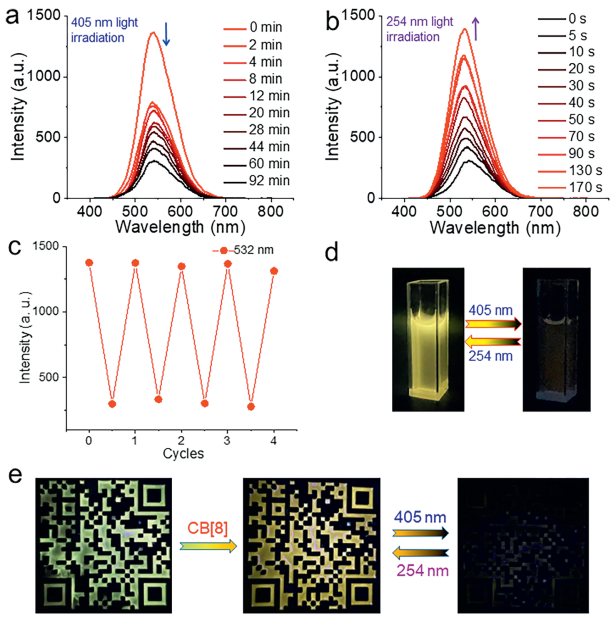

Fig. 3. (a) Fluorescence spectral variation of (*E*)-SSB-(*E*)-FMR/CB[8] (2.0×10^{-5} mol/L) upon 405 nm light irradiation. (b) Fluorescence photographs of (*E*)-SSB-(*E*)-FMR/CB[8] under 365 nm UV light upon alternating visible-light (405 nm) and UV (254 nm) irradiation. (c) Fluorescence spectral variation of the resultant sample **a** upon 254 nm light irradiation. (d) Fluorescence spectra variation of (*E*)-SSB-(*E*)-FMR upon alternating visible-light (405 nm) and UV (254 nm) irradiation; Inset: Fluorescence intensity changes at 532 nm of (*E*)-SSB-(*E*)-FMR observed upon alternating visible-light (405 nm) and UV (254 nm) irradiation. (e) QR code anti-counterfeiting adjustment induced by addition of CB[8] and distinct light ($\lambda_{ex} = 400$ nm).

aforementioned process could be repeated for many times originated from good fatigue resistance, achieving light-triggered reversible information hiding and recognition and multi-encrypted anti-counterfeiting.

Possessing strong fluorescence, high PLQY, good water-solubility and outstanding fluorescence switching reversibility, the applications of (*E*)-SSB-(*E*)-FMR/CB[8] was further explored in targeted bioimaging. 3T3 cells were chosen to be co-stained with the (*E*)-SSB-(*E*)-FMR/CB[8] assembly and commercially acquired lysosome staining dye LysoBlue for only 0.5 h in the dark. Afterwards, confocal laser scanning microscopy was utilized to inspect the intracellular distribution of the assembly. As displayed in Fig. 4c, the merged image of green (*E*)-SSB-(*E*)-FMR/CB[8] (Fig. 4b) and blue LysoBlue (Fig. 4a) manifested that the assembly and LysoBlue were absolutely co-located in the same location, exhibiting that the supramolecular assembly developed by us realized precise lysosomal targeting imaging in living cells. In addition, outstanding reversible fluorescence photoswitching peculiarity gave us an idea to conduct photocontrolled lysosomal targeting imaging. As discerned in Fig. 4d, the strong green fluorescence in lysosomes was quenched upon 405 nm laser irradiation (built-in light source) for 5 min and subsequently the original fluorescence was completely recovered by 254 nm light irradiation (external light source) for 4 s. Besides, we performed several irradiation cycle experiments, and no apparent decay was observed, implying good anti-fatigue performance for the photoresponsive lysosomal targeting imaging switching. Furthermore, it was indispensable to evaluate the cytotoxicity of the assembly. 3T3 cells were incubated with the assembly for 24 h, and then we examined the cell viability by MTT assays. When the concentration of the assembly was under 5×10^{-6} mol/L ($[(E)\text{-SSB-}(E)\text{-FMR}] = [\text{CB[8]}] = 5 \times 10^{-6}$ mol/L), the toxicity to 3T3 cells was completely negligible (Fig. 4e). The supramolecular intelligent photoluminescence material fabricated

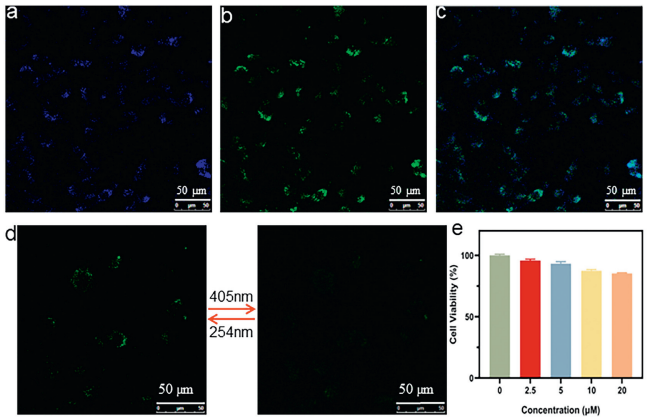

Fig. 4. Confocal fluorescence images of 3T3 cells co-stained with (*E*)-SSB-(*E*)-FMR/CB[8] ([(*E*)-SSB-(*E*)-FMR] = [CB[8]] = 5×10^{-6} mol/L) and LysoBlue (5×10^{-6} mol/L) for 0.5 h: (a) LysoBlue (Ex. 405 nm, Em. 425 nm); (b) (*E*)-SSB-(*E*)-FMR/CB[8] (Ex. 405 nm, Em. 532 nm). (c) Merged image of (a) and (b); (d) The evolution and reversibility of confocal fluorescence images of 3T3 cells co-stained with (*E*)-SSB-(*E*)-FMR/CB[8] in the same area upon alternate 405 nm and 254 nm laser irradiation. (e) Relative cell viabilities of (*E*)-SSB-(*E*)-FMR/CB[8] at different concentrations.

by us owned several major advantages in lysosomal targeting imaging as follows: (1) Low concentration needed (5×10^{-6} mol/L) comparable to commercial dyes; (2) more accurate positioning based on fluorescence photoswitching function; (3) good photoluminescence performance. Therefore, we herein reported the first stiff-stilbene-based supramolecular photoluminescence material with the function of photo-switching lysosomal targeting imaging, to the best of our knowledge.

In summary, we designed and synthesized a stiff-stilbene-modified fluorescence molecular rotor (*E*)-SSB-(*E*)-FMR, possessing both photoisomerization and AIE characteristics. Stiff-stilbene conjugated system was extended through introduction of FMR unit, and its absorption band was shifted bathochromically to visible region, led to the occurrence of visible light-induced photoisomerization from (*E*)-from to (*Z*)-configuration. Nevertheless, it suggested unsatisfactory reversibility. To our delight, (*E*)-SSB-(*E*)-FMR could assemble with CB[8] to form photoinduced 2:2 quaternary supramolecular assembly (*E*)-SSB-(*E*)-FMR/CB[8] with good reversibility, where intervention of macrocyclic host CB[8] greatly improved reversibly photoisomerized fatigue resistance of the guest and enhanced its fluorescence intensity and quantum yield. More significantly, the supramolecular assembly (*E*)-SSB-(*E*)-FMR/CB[8] exhibited outstanding fluorescence photoswitching behaviors and performance, which was further applied in tunable QR code anti-counterfeiting induced by host and distinct light. Besides, the water-soluble photoluminescent supramolecular assembly also possessed photoswitching lysosomal targeting imaging function. The study provided a simple and feasible supramolecular method for improving efficiently reversibility of stiff-stilbenes and construction of stiff-stilbene-based intelligent photoluminescence materials with excellent performance.

Declaration of competing interest

The authors declare that they have no known competing financial interests or personal relationships that could have appeared to influence the work reported in this paper.

Acknowledgments

We thank National Natural Science Foundation of China (No. 21801063), Top-Notch Talents Program of Henan Agricultural University (No. 30501049), Natural Science Foundation of Henan Province (No. 232300420132) and the Merit Funding for the Oversea Staff of Henan Province for financial support.

Supplementary materials

Supplementary material associated with this article can be found, in the online version, at doi:10.1016/j.cclet.2023.109403.

References

[1] D.S. Guo, Y. Liu, Acc. Chem. Res. 47 (2014) 1925–1934.
[2] Y. Zhang, L. Wang, J. Wang, S. Xin, X. Sheng, Chin. Chem. Lett. 32 (2021) 1902–1906.
[3] F. Soto, E. Karshalev, F. Zhang, et al., Chem. Rev. 122 (2022) 5365–5403.
[4] M. Su, Y. Song, Chem. Rev. 122 (2022) 5144–5164.
[5] H.K. Bisoyi, Q. Li, Chem. Rev. 122 (2022) 4887–4926.
[6] Y. Zhao, S. Song, X. Ren, et al., Chem. Rev. 122 (2022) 5604–5640.
[7] T. Cui, G. Liu, W. Zhang, et al., Chin. Chem. Lett. 32 (2021) 357–361.
[8] L. Miao, X. Zhu, G. Liu, et al., Chin. Chem. Lett. 34 (2023) 107921.
[9] T. Xiao, J. Wang, Y. Shen, et al., Chin. Chem. Lett. 32 (2021) 1377–1380.
[10] T. Xiao, W. Zhong, L. Zhou, et al., Chin. Chem. Lett. 30 (2019) 31–36.
[11] C. Wang, Y.M. Zhang, H. Li, et al., Chin. Chem. Lett. 33 (2022) 2447–2450.
[12] L. Zhang, Y.M. Zhang, G.X. Liu, Y. Liu, Chin. Chem. Lett. 30 (2019) 120–122.
[13] Z. Cao, D. Wu, M. Li, et al., Chin. Chem. Lett. 33 (2022) 1533–1536.
[14] M. Chen, M. Zhong, J.A. Johnson, Chem. Rev. 116 (2016) 10167–10211.
[15] D.H. Qu, Q.C. Wang, Q.W. Zhang, et al., Chem. Rev. 115 (2015) 7543–7588.
[16] G. Liu, Y.M. Zhang, X. Xu, et al., Adv. Opt. Mater. 5 (2017) 1700770.
[17] G. Liu, Y.M. Zhang, X. Xu, et al., Adv. Opt. Mater. 5 (2017) 1700149.
[18] S. Lin, K.G. Gutierrez-Cuevas, X. Zhang, et al., Adv. Funct. Mater. 31 (2021) 2007957.
[19] L. Wang, Q. Li, Chem. Soc. Rev. 47 (2018) 1044–1097.
[20] M. Kathan, S. Hecht, Chem. Soc. Rev. 46 (2017) 5536–5550.
[21] J. de Jong, J.E. Bos, S.J. Wezenberg, Chem. Rev. 123 (2023) 8530–8574.
[22] J. Volarić, W. Szymanski, N.A. Simeth, B.L. Feringa, Chem. Soc. Rev. 50 (2021) 12377–12449.
[23] R. Costil, M. Holzheimer, S. Crespi, et al., Chem. Rev. 121 (2021) 13213–13237.
[24] K. Imato, A. Sasaki, A. Ishii, et al., J. Org. Chem. 87 (2022) 15762–15770.
[25] G. Liu, J. Leng, Q. Zhou, et al., Dyes Pigments 203 (2022) 110361.
[26] L. Yang, Y. Li, H. Zhang, et al., Chin. Chem. Lett. 34 (2023) 108108.
[27] M.P. O'Hagan, S. Haldar, M. Duchi, et al., Angew. Chem. Int. Ed. 58 (2019) 4334–4338.
[28] G. Liu, Y.M. Zhang, C. Wang, Y. Liu, Chem. Eur. J. 23 (2017) 14425–14429.
[29] G. Liu, X. Xu, X. Dai, et al., Mater. Horiz. 8 (2021) 2494–2502.
[30] S.J. Barrow, S. Kasera, M.J. Rowland, et al., Chem. Rev. 115 (2015) 12320–12406.
[31] H. Nie, Z. Wei, X.L. Ni, Y. Liu, Chem. Rev. 122 (2022) 9032–9077.
[32] Y.X. Wang, Y.M. Zhang, Y. Liu, J. Am. Chem. Soc. 137 (2015) 4543–4549.
[33] R. Schmidt, M. Stolte, M. Grüne, F. Würthner, Macromolecules 44 (2011) 3766–3776.
[34] X. Yang, R. Wang, A. Kermagoret, D. Bardelang, Angew. Chem. Int. Ed. 59 (2020) 21280–21292.
[35] J. Wang, Z. Huang, X. Ma, H. Tian, Angew. Chem. Int. Ed. 59 (2020) 9928–9933.